Journal of proteome research

Article

pubs.acs.org/jpr

Proteome Analysis Unravels Mechanism Underling the Embryogenesis of the Honeybee Drone and Its Divergence with the Worker (*Apis mellifera lingustica*)

Yu Fang, Mao Feng, Bin Han, Yuping Qi, Han Hu, Pei Fan, Xinmei Huo, Lifeng Meng, and Jianke Li*

Institute of Apicultural Research/Key Laboratory of Pollinating Insect Biology, Ministry of Agriculture, Chinese Academy of Agricultural Sciences, Beijing, 100093, China

Supporting Information

ABSTRACT: The worker and drone bees each contain a separate diploid and haploid genetic makeup, respectively. Mechanisms regulating the embryogenesis of the drone and its mechanistic difference with the worker are still poorly understood. The proteomes of the two embryos at three time-points throughout development were analyzed by applying mass spectrometry-based proteomics. We identified 2788 and 2840 proteins in the worker and drone embryos, respectively. The age-dependent proteome driving the drone embryogenesis generally follows the worker's. The two embryos however evolve a distinct proteome setting to prime their respective embryogenesis. The strongly expressed proteins and pathways related to transcriptional−translational machinery and morphogenesis at 24 h drone embryo relative to the worker, illustrating the earlier occurrence of morphogenesis in the drone than worker. These morphogenesis differences remain through to the middle−late stage in the two embryos. The two embryos employ distinct antioxidant mechanisms coinciding with the temporal-difference organogenesis. The drone embryo's strongly expressed cytoskeletal proteins signify key roles to match its large body size. The RNAi induced knockdown of the ribosomal protein offers evidence for the functional investigation of gene regulating of honeybee embryogenesis. The data significantly expand novel regulatory mechanisms governing the embryogenesis, which is potentially important for honeybee and other insects.

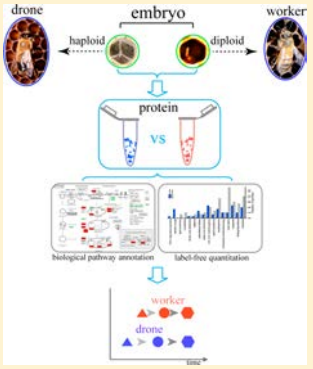

KEYWORDS: *honeybee, worker, drone, embryo, proteome*

1. INTRODUCTION

As a eusocial insect, a honeybee (*Apis mellifera*) colony has three different casts, queen, worker, and drone bees. The worker and drone are derived from fertilized (diploid) and unfertilized (haploid) eggs, respectively, laid by queen bees.[1−3] The distinct genetic background between the worker and drone renders a specific development trajectory and wide spectrum of social behaviors in the honeybee community.[1] An adult worker bee hatches out from an egg after a development of 21 days, whereas a drone bee needs about 24 days. Moreover, the worker bees engage in virtually all the labor activities, such as cleaning the hive, tending the brood, foraging for food, and building cells,[4,5] but the quite limited function of drone bees is to produce sperm for mating with a virgin queen.[3] Accordingly, relative to the dominant female worker in the colony, the drone bees are physiologically lacking hypopharyngeal glands, wax glands, and most of the structures to collect food but are equipped with elaborate organs for powerful sensing and flying capacity[6] to find a virgin queen in the open air and to compete with hundreds of other drones to mate with her.[7]

Embryogenesis is the first stage in honeybee life circle, during which the rudimentary organs of adult bees are formed.[2,3] Accumulating evidence demonstrates that the embryo is the ideal model for honeybee genetic modification. Several physiological characters of the honeybee embryo make it an ideal stage of development for study, such as a thin chorion, a relatively easy maintenance process of the ambient environment (34 °C temperature, 80% relative humidity) during development, and the ability to easily puncture a hole on the shell and still have it develop normally under lab conditions.[2,3] Because of these biological merits, genetic manipulations of the honeybee embryo have been documented in the areas of transplantation of nuclear materials[8] and RNA interference.[9−11] Recently, the in vitro cultivation of the embryonic cell[12−17] has offered a potential venue to study one target gene or protein that regulates the embryonic development of the honeybee.

Toward the above-mentioned goals, unraveling the molecular mechanism driving the embryonic development is the first initial step. Apart from the morphological description of worker embryogenesis,[18−20] only a few works have been reported for the investigation into the honeybee embryogenesis of worker or drone.[21,22] Mechanistic differences between the worker and drone embryogenesis at the molecular level are still lacking.

The recently updated honeybee genome has significantly expanded its proteome with over 15 000 annotated proteins.[23] This offers a crucially important resource for the honeybee proteome study. Moreover, MS-based proteomics allows the

Received: July 6, 2015

DOI: 10.1021/acs.jproteome.5b00625
J. Proteome Res. XXXX, XXX, XXX−XXX

identification and quantification of several thousand proteins and provides a treasure trove for gaining a better understanding of the molecular details in the brain,[24] embryo,[22,25] larvae,[26] hypopharyngeal gland,[27,28] saliva gland,[29] and hemolymph[30] of the honeybee. Despite the previous works on dissecting the molecular mechanism of the worker and drone embryogenesis at the proteome level,[22,25] the previous techniques have a limited depth of proteome coverage in the honeybee embryos, particularly for the drone. This limitation hinders a deeper understanding of the mechanisms of embryogenesis in the drone. In addition, the drone's mechanistic divergence with the worker has yet to be addressed. Therefore, in-depth molecular decipherment of the drone embryogenesis and its difference with the worker have received considerable interest because of their biological significance of honeybee developmental biology. To better understand the distinct regulatory mechanisms underlying embryogenesis of the worker and drone bees, we report here an unprecedented depth of the proteome in the honeybee embryos, decipher molecular details that regulate the drone embryogenesis, and find a wide range of differences between the worker and drone.

2. MATERIALS AND METHODS

2.1. Chemical Reagents

Unless otherwise specified, all chemicals were bought from Sigma-Aldrich (St. Louis., MO).

2.2. Sampling and Protein Preparation

The honeybee (*A. m. lingustica*) colonies were raised at the Institute of Apicultural Research, Chinese Academy of Agricultural Science, Beijing, China. Eggs were sampled from worker and drone combs at 24, 48, and 72 h of age according to our previously described method.[25] For each time point, 1000 eggs were collected from five colonies and stored at −80 °C until further analysis. Three independent biological replicates were produced per time-point.

Protein extraction was carried out according to our previous method.[22] Briefly, frozen egg samples were homogenized in lysis buffer (8 M urea, 2 M thiourea, 4% 3-[(3-cholamidopropyl)dimethylammonio]-1-propanesulfonate (CHAPS), 20 mM Tris-base, 30 mM dithiothreitol (DTT), 2% Biolyte pH 3−10, 1 mg/10 μL) on ice, followed by centrifuging at 15 000 × *g* for 15 min at 4 °C to remove insoluble fractions. The supernatant was precipitated with ice-cold acetone at −20 °C for 30 min and then centrifuged twice at 15 000 × *g* for 10 min at 4 °C to pellet protein. Finally, the precipitate was extracted at room temperature for 10 min and dissolved in 40 mM $(NH_4)HCO_3$. Protein concentrations were determined by the Bradford assay.[31]

2.3. Trypsin Digestion and MS Analysis

Denatured proteins were reduced with DTT (final concentration 10 mM) and alkylated with iodoacetamide (final concentration 50 mM) to prevent reformation of disulfide bonds. Then the samples were digested using sequencing grade modified trypsin (Promega, Medison, WI) and incubated for 14 h at 37 °C. Finally, peptides were pooled and dried using a Speed-Vac system (RVC 2−18, Marin Christ) for MS/MS analysis.

The digested peptides were resuspended in 15 μL of loading buffer (0.1% formic acid) prior to MS analysis. Then 10 μL of peptides was subjected to LC−MS/MS analysis using an Easy-nLC 1000 (Thermo Fisher Scientific, Rockford, IL) coupled to a Orbitrap Elite MS (Thermo Fisher Scientific, Rockford, IL) via a nanoelectrospray ion source (spray voltage 2.3 kV, capillary temperature 275 °C and S-Lens RF 55%). The tryptic digests were loaded onto an Easy-spray trap column packed with 2 μm C18 (100 Å, 75 μm x 50 cm, Thermo Fisher Scientific) in the loading solvent (0.1% formic acid, 2% acetonitrile in H_2O). Peptides were separated on the analytical column packed with 3 μm C18 (100 Å, 75 μm x 15 cm, Thermo Fisher Scientific) using a 130 min gradient from 3−30% acetonitrile (0.1% formic acid) with a flow of 250 nL/min.

The mass spectrometer was run in positive ion mode, MS scan control was done using the Xcalibur software (Version 2.2, Thermo Fisher Scientific), and MS data acquisition was carried out in a data-dependent manner. Dynamic exclusion was enabled with a repeat count of 1 and exclusion duration of 30 s. MS1 precursor scan (m/z 300−2000) acquisition was performed in the orbitrap using a nominal resolution of 30 000 at m/z 400 followed by MS2 fragmentation of top 20 most intensity multiply charged precursor ions, which were fragmented by higher energy collisional dissociation (HCD) with a normalized fragmentation energy of 35%. MS2 scans (m/z 100−2000) were acquired in the orbitrap mass analyzer using a resolution setting of 15 000 at m/z 400 and start from m/z 100.

2.4. Protein Identification

The MS/MS spectra were searched using PEAKS search engine (version 7.0, Bioinformatics Solutions Inc.) against the sequence database generated from protein sequences of *Apis mellifera* (downloaded October, 2014) and the common contaminants, totaling 21 777 entries.[32] The database search parameters were: precursor ion and MS/MS tolerances, 20 ppm and 0.05 Da; enzyme specificity, trypsin; maximum missed cleavages, 2; fixed modification, carbamidomethyl (C, + 57.02); and variable modification, oxidation (M, + 15.99). The fusion strategy of target and decoy sequence was used to control false discovery rate (FDR) at 1% at the peptide level for protein identification. Only a protein with at least one unique peptide with identification of at least two spectra was considered to be identified.

2.5. Label-Free Quantitation of Protein Abundance

To quantify the level alteration of protein abundance between the worker and drone embryos at three time-points of development, and the protein abundance changes across the three time-points of growth of worker and drone bees, the label-free strategy was performed by Progenesis LC−MS software (version 4.1, Nonlinear Dynamics, UK). Triplicates of each technical sample were subjected to software for subsequent quantitation analysis. After the data quality control by alignment of retention time of each MS run, one run was selected as reference, followed by automatic feature matching for all runs with further manual editing to correct the mismatched and unmatched feature detection. Thereafter, the abundance of discriminatory peptides was the sum of the peak areas within the isotope boundaries of the corresponding feature. The expression level of each protein was calculated in terms of its peptide ion abundance of three replicates. Then the normalization was performed to calibrate data between different sample runs and correct the systematic experimental variation when running samples. The differences in protein expression levels between each time point throughout the selected development stages were determined by one-way analysis of variance (ANOVA) using a q-value for multiple tests.

DOI: 10.1021/acs.jproteome.5b00625
J. Proteome Res. XXXX, XXX, XXX−XXX

The differences of protein abundance level were taken as statistically significant when they contained at least two-fold changes and $p < 0.05$.

2.6. Bioinformatics Analysis

The functional gene ontology (GO) category was annotated using Blast2GO PRO[33] to assign the identified proteins into specific GO terms.

To enrich the statistically significant biological pathway of the identified proteins, it was analyzed by KEGG orthology-based annotation system (KOBAS, http://kobas.cbi.pku.edu.cn),[34] and this essentially followed previously described protocol elsewhere.[25]

To gain additional insight into possible functional connections between the identified proteins, the protein−protein interaction (PPI) networks were constructed with GeneMANIA, which uses a large set of functional association data including protein and genetic interactions.[35] The integrated known and predicted PPI data sets from *Drosophila melanogaster* were entered into GeneMANIA. Then the software performed a FDR-corrected hypergeometric test for GO category enrichment in the input data set compared to the background set of GO annotations in the entire *D. melanogaster* genome. The networks of predicted, genetic, and physical interactions were enabled. The top 20 related genes and at most 20 attributes are displayed using GO biological process-based weighting. Proteins were grouped according to their GO annotations involvement in biological processes, and networks were visualized in Cytoscape.

To create an expressional profile of differentially expressed proteins, the unsupervised hierarchical cluster of the differentially expressed proteins was performed by gene cluster 3.0[36] using uncentered Pearson correlation and average linkage, and it was visualized by Java Treeview software.[37]

2.7. Quantitative Real-Time Polymerase Chain Reaction (qPCR)

To examine the consistency of the protein expression and its encoding gene, 20 key proteins in the PPI networks were selected for qPCR analysis. RNA was isolated from 24, 48, and 72 h old embryos of workers and drones (TRIzol reagent, Invitrogen, CA) and quantified with a NanoDrop ND-1000 spectrophotometer (NanoDrop Technologies Inc.). Then cDNA was generated using Reverse Transcriptase kit reagents (Transgen, China) according to the manufacturer's instructions. Differentially expressed proteins from the PPI networks were selected for qPCR analysis (primers seen, Supplemental Table S1). PCR amplification was performed by iQ5Multicolor Real-Time PCR Detection System (Bio-Rad, Hercules, CA) following our previous protocol,[22] and glyceraldehyde-3-phosphate dehydrogenase (GAPDH) was used as a reference gene (internal control). Triplicate was produced in each sample. The level of gene expression was calculated by ΔΔCt method.[38] An error probability $p < 0.05$ was considered statistically significant gene expression by one-way ANOVA (SPSS version 16.0, SPSS, Inc.) using Duncan's multiple-range test.

2.8. Western-Blotting Analysis

To validate the label-free MS data, Western-Blotting analysis of honeybee embryos was done as previously described[39] using the ECL (enhanced chemiluminescence). We selected three differentially expressed proteins for the validation. Commercially available primary antibodies were obtained from Abcam (Cambridge, MA), and the others were prepared by Genecreat (Wuhan, China). The primary rabbit polyclonal antibodies were anti-60S ribosomal protein L36 (RpL36), antilachesin-like isoform X1 (Lach), and antisex-regulated protein janus-A-like (janA) at dilutions of 1:5000, 1:4000, and 1:6000, respectively; the secondary antibody was horseradish peroxidase-conjugated goat antirabbit at a dilution of 1:5000. About 10 μg of protein samples was separated by stacking (4%) and separating (12%) sodium dodecyl phosphate polyacrylamide gel electrophoresis (SDS-PAGE) gels, and each sample was run in triplicates. Protein was transferred to nitrocellulose membranes using a dry blotting apparatus (iBlot Gel Transfer System, Invitrogen, CA). The bands of protein were visualized by chemiluminescence. Bands were quantified by densitometry using a Quantity-one image analysis system (Bio-Rad, Hercules, CA), and the protein abundance was normalized by GAPDH. The student *t* test was used for statistical analysis of protein abundance.

2.9. RNA Interference

The DNA sequences of protein RpL36 with T7 promoter were synthesized by Genecreat (sequences in Supplemental Table S2). The double-stranded RNA (dsRNA) was then prepared using the MEGAscript RNA kit (Ambion) following the manufacturer's protocol. The injections of dsRNA were performed with a microinjection system (ONO-301D, Narishige Co., Ltd., Japan) and an ordinary dissecting microscope. The injection pipettes were pulled by micropipette puller (PN-31, Narishige Co., Ltd., Japan) with the parameter: heater 62.8 °C, magnet sub 28.2, magnet main 88.9. dsRNA was injected at 2.5 μg/μL in H_2O into freshly laid honeybee eggs (5 nL injected into each embryo), while the equal volume of sterile water was injected as a control. The injected embryos were hatched at 34 °C and 80% humidity in the incubator (BSC-250, Boxun industry and commerce Co., Ltd., China) and harvested at 24, 48, and 72 h. The survival dsRNA injected embryos was sampled for Western-Blotting and qPCR analyses as described earlier.

3. RESULTS

3.1. Time-Coursed Proteome of Drone Embryo

During the complete course of drone embryonic development, 1560, 2055, and 1819 proteins were identified at the ages of 24, 48, and 72 h, representing 2840 nonredundant proteins (Figure 1, Supplemental Tables S3−S5). Of the 2840 proteins, they were mainly implicated in 16 functional GO terms on the basis of biological processes (Supplemental Table S6). The major

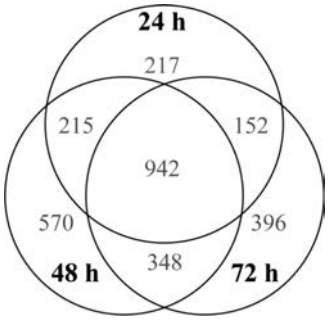

Figure 1. A global proteomics view of the drone honeybee's embryo (*A.m.ligustica*) across the three time points. Venn diagrams indicate the numbers of common and unique proteins identified in the drone honeybee's embryo at 24, 48, and 72 h.

DOI: 10.1021/acs.jproteome.5b00625
J. Proteome Res. XXXX, XXX, XXX−XXX

represented categories were proteins related to transcription (14.9%), followed by proteins associated with transporter (13.1%), folding/degradation (9.5%), carbohydrate metabolism/energy (9.2%), and translation (8.5%). Noticeably, 942 proteins (33% of 2840) were shared across the three differently aged embryos (Figure S1). Among them, the major represented GO terms were proteins associated with translation (14.8%), folding/degradation (13.8%), transporters (12.9%), carbohydrate metabolism/energy (12.3%), and transcription (9.0%).

To identify the key biological pathways during the embryogenesis of the honeybee drone, all of 1560, 2055, and 1819 proteins were successfully annotated to the KEGG database at 24, 48, and 72 h, respectively (Supplemental Tables S7–S9). Five shared biological pathways were significantly enriched in the three ages of embryos: ribosome, proteasome, citrate cycle, carbon metabolism, and the biosynthesis of amino acids. Moreover, pyruvate metabolism ($p = 9.0 \times 10^{-4}$), starch and sucrose metabolism ($p = 6.0 \times 10^{-4}$), cysteine and methionine metabolism ($p = 8.3 \times 10^{-3}$), glyoxylate and dicarboxylate metabolism ($p = 8.0 \times 10^{-3}$), and pentose/glucuronate interconversions ($p = 7.0 \times 10^{-3}$) were specifically enriched pathways in the 24 h embryo. Phagosome ($p = 5.1 \times 10^{-4}$), aminoacyl-tRNA biosynthesis ($p = 7.2 \times 10^{-3}$), phototransduction ($p = 3.2 \times 10^{-3}$), and valine/leucine/isoleucine degradation ($p = 1.5 \times 10^{-2}$) were exclusively enriched in the 48 h embryo, and circadian rhythm ($p = 1.6 \times 10^{-5}$) was uniquely enriched in the 72 h embryo (Figure 2).

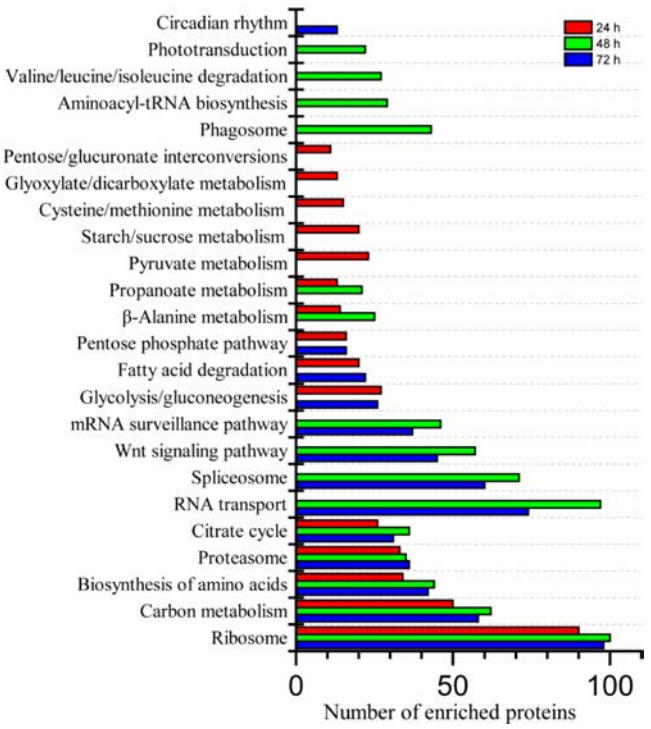

Figure 2. Biological pathway enrichment of identified proteins in the embryos of honeybee drones (*A.m.ligustica*). Comparison of enriched biological pathways of the identified proteins in the embryo of honeybee drones (*A.m.ligustica*) aged at 24, 48, and 72 h. Significantly enriched pathways are analyzed by KOBAS.[35] The pathway enrichment is conducted by a hypergeometric statistic test. The Benjamini and Hochberg FDR correction is used to correct the probability values, and only those corrected at $p < 0.05$ are considered as statistically significant enriched pathways.

Quantitatively, 510 proteins significantly changed their level of expression (fold change ≥ 2 and $p < 0.05$) during the drone embryogenesis, representing ∼18% of the 2840 proteins (Supplemental Table S10). These differential proteins were abundantly associated with folding/degradation, carbohydrate metabolism/energy, transporters, and transcription.

To visualize expression profiles during the drone embryogenesis, the 510 differential proteins were clustered based their abundance levels. Of the 53, 374, and 83 proteins upregulated in three respective aged embryos, functional classes of transporter, transcription, and translation were overrepresented at 24 h; carbohydrate metabolism/energy and folding/degradation were predominant at 48 h, and transcription and translation categories were overrepresented at 72 h (Figure 3,

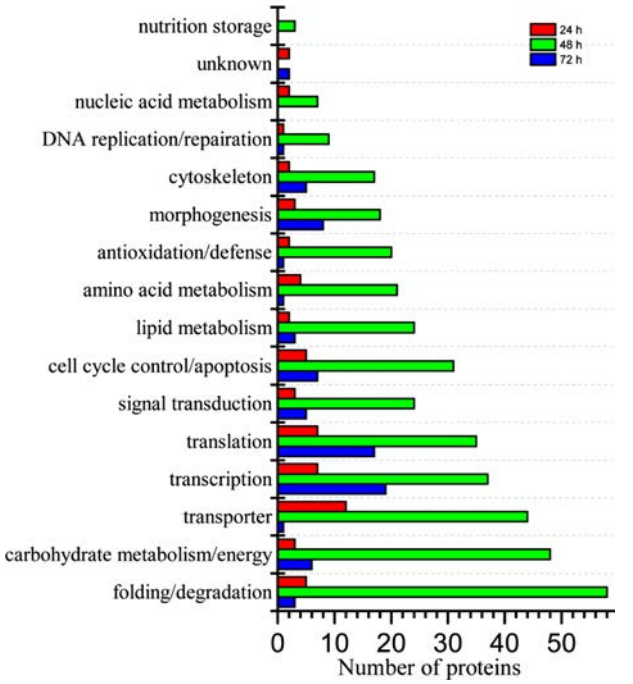

Figure 3. Comparison of the upregulated proteins by their functional class at three developmental stages of the honeybee drone (*A.m.ligustica*) embryo. Proteins are classified based on the biological process of GO using Blast2GO PRO.[36] Color codes denote the three aged samples.

Supplemental Table S10). Regarding the proteins with elevated levels of abundance expressed in the PPI network, the functional category of cell maturation (q-value = 2.7×10^{-2}) was enriched at 24 h (Figure S2A); ribosome (q-value = 1.0×10^{-14}), ubiquitin-dependent protein catabolic process (q-value = 6.8×10^{-10}), oocyte development (q-value = 5.6×10^{-9}), programmed cell death (q-value = 2.1×10^{-8}), cellular response to DNA damage stimulus (q-value = 2.8×10^{-8}), and macromolecular complex assembly (q-value = 1.6×10^{-5}) were significantly found at the middle stage (Figure S2B); and polytene chromosome (q-value = 4.9×10^{-4}) and chromatin organization (q-value = 2.8×10^{-2}) were significantly enriched at 72 h embryo (Figure S2C).

3.2. Proteome Difference between the Worker and Drone at 24 h

At 24 h of age, of the 1903 proteins (1477 identified in worker and 1526 in drone), 1100 proteins (58%) were shared between the worker and drone (Figure S3A, Supplemental Table S11);

DOI: 10.1021/acs.jproteome.5b00625
J. Proteome Res. XXXX, XXX, XXX−XXX

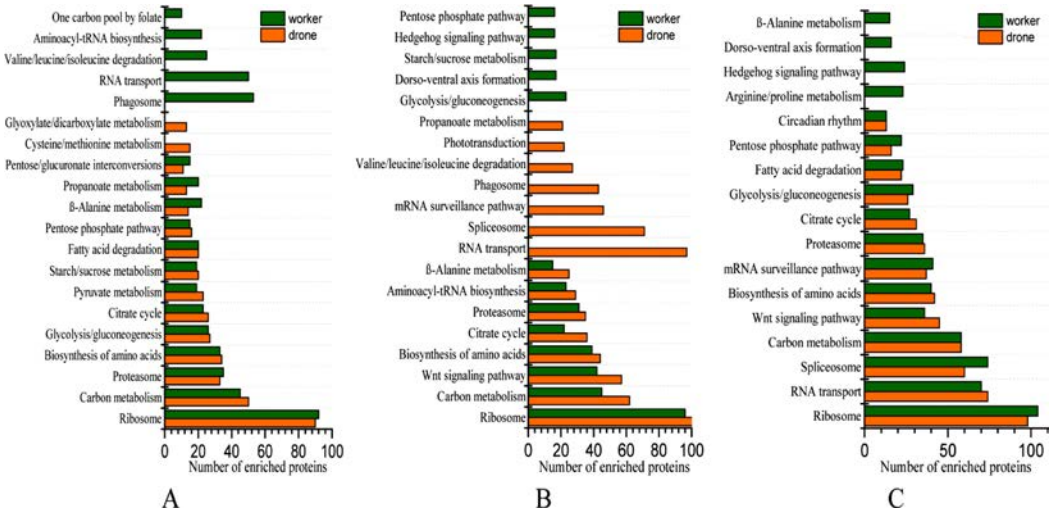

Figure 4. Comparison of enriched biological pathways of the identified proteins in the embryo of the honeybee worker and drone (*A.m.ligustica*) at the ages of 24 h (A), 48 h (B), and 72 h (C), respectively.

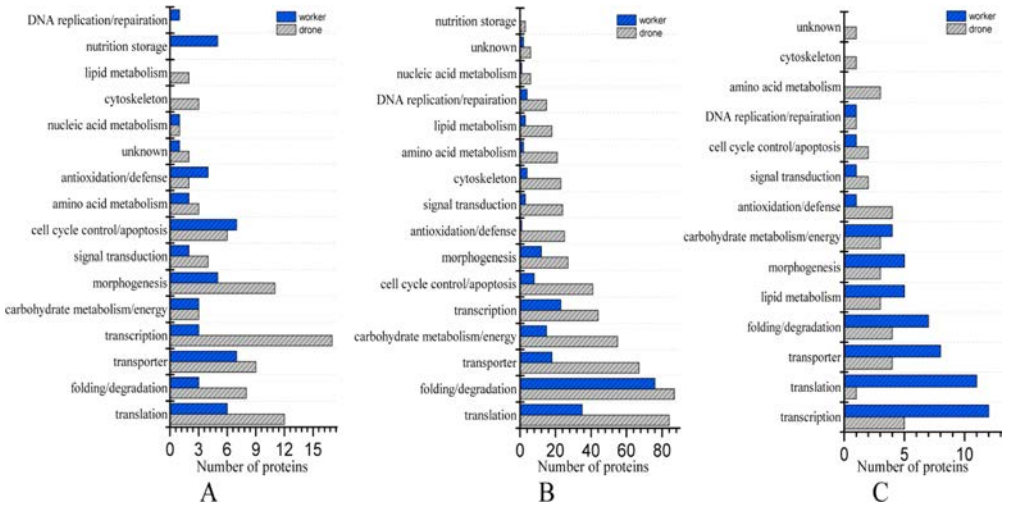

Figure 5. Comparison of the upregulated proteins by their functional classes between the honeybee worker and drone (*A.m.ligustica*) at the embryonic developmental stages at the embryo ages of 24 h (A), 48 h (B), and 72 h (C), respectively.

they were mainly implicated in transporter, translation, folding/degradation, carbohydrate metabolism/energy, and transcription, and significantly enriched in 13 shared pathways (Figure 4A, Supplemental Tables S7 and S12). Noticeably, five pathways were uniquely enriched in the worker embryo: aminoacyl-tRNA biosynthesis ($p = 4.1 \times 10^{-2}$), one carbon pool by folate ($p = 2.4 \times 10^{-2}$), valine/leucine/isoleucine degradation ($p = 7.6 \times 10^{-4}$), RNA transport ($p = 4.1 \times 10^{-2}$), and phagosome ($p = 3.6 \times 10^{-10}$); while two pathways were exclusively enriched in the drone embryo, glyoxylate/dicarboxylate ($p = 5.0 \times 10^{-2}$) and cysteine/methionine ($p = 5.0 \times 10^{-2}$) metabolism (Figure 4A, Supplemental Tables S7 and S12). Moreover, the worker expressed a higher number of proteins involved in lipid metabolism, and fewer proteins were implicated in cell cycle control/apoptosis and morphogenesis than those in the drone (Figure S4A, Supplemental Tables S3 and S11). Among the 1903 proteins, 120 proteins were differentially expressed (fold change ≥ 2 and $p < 0.05$), of which 49 were upregulated in the worker and 71 in the drone. For these proteins with altered abundance, functional class of morphogenesis, transcription, translation, and transporter in the drone embryo were highly represented relative to the worker (Figure 5A, Supplemental Table S13). Still, the upregulated proteins in the worker embryo were significantly implicated in a positive regulation of macromolecule biosynthetic process (q-value $= 2.6 \times 10^{-2}$) in the interaction network (Figure 6A). However, four terms were significantly enriched in the drone such as macromolecular complex assembly (q-value $= 5.0 \times 10^{-3}$), microtubule (q-value $= 3.8 \times 10^{-2}$), eukaryotic translation initiation factor 3 complex (q-value $= 1.8 \times 10^{-2}$), and neuron projection guidance (q-value $= 2.7 \times 10^{-2}$) (Figure 6D).

3.3. Proteome Difference between the Worker and Drone at 48 h

At 48 h, 2716 proteins were found in worker and drone embryos, of which 1332 were identified by both (Figure S3B, Supplemental Tables S4 and S14). Five pathways (pentose phosphate pathway, hedgehog signaling pathway, starch and sucrose metabolism, dorsal-ventral axis formation, and glycolysis/gluconeogenesis) were significantly and uniquely enriched in the worker (Figure 4B, Supplemental Tables S8 and S15). Seven pathways (phagosome, phototransduction, prop-

DOI: 10.1021/acs.jproteome.5b00625
J. Proteome Res. XXXX, XXX, XXX−XXX

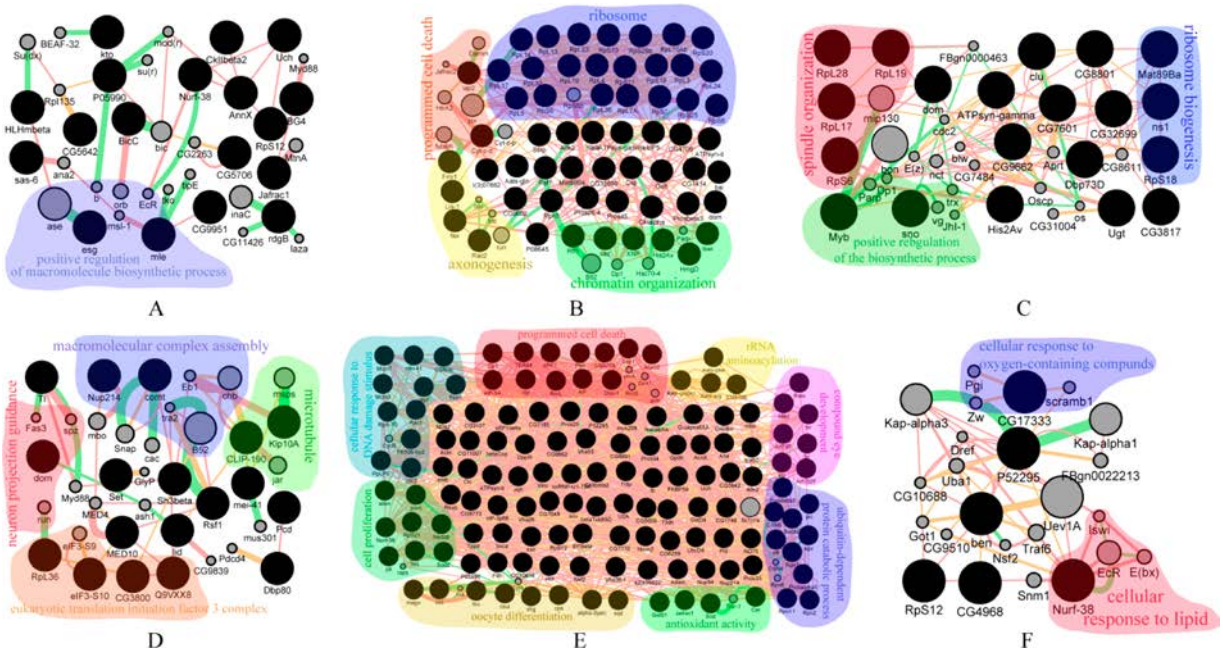

Figure 6. PPI network of the upregulated proteins expressed in each embryonic development stage of the honeybee worker and drone (*A.m.ligustica*). The visualizations of the interactions between the upregulated proteins in the top enriched pathways is rendered using the Genemania plugin within Cytoscape.[36] The software performed a FDR-corrected hypergeometric test for GO category enrichment in the input data set compared to the background set of GO annotations in the entire *D. melanogaster* genome. The networks of predicted, genetic, and physical interactions are enabled. The top 20 related genes and at most 20 attributes are displayed using GO biological process-based weighting. Proteins are grouped according to their GO annotation involvement in biological processes. PPI networks in honeybee worker and drone embryos aged at 24 h (A), 48 h (B), and 72 h (C), respectively.

anoate metabolism, valine/leucine/isoleucine degradation, mRNA surveillance pathway, spliceosome, and RNA transport) were exclusively enriched in the drone. Eight other pathways (citrate cycle, proteasome, ribosome, β-alanine metabolism, aminoacyl-tRNA biosynthesis, biosynthesis of amino acids, wnt signaling pathway, and carbon metabolism) were shared by the worker and drone (Figure 4B, Supplemental Tables S8 and S15). Of those 2716 proteins at 48 h, 1332 proteins (49%) were present in both embryos (Figure S3B), which were mainly involved in transporter, translation, folding/degradation, carbohydrate metabolism/energy, and transcription. Moreover, among the 625 proteins changing the level of expression between the worker and drone, 151 were upregulated in the worker and 474 in the drone (Figure 5B, Supplemental Table S16). The enhanced level of proteins associated with folding/degradation, translation, transporter, and transcription were commonly overrepresented in both worker and drone, and the numbers of each protein class elevated in expression during the development of drone embryo were larger than that in the workers (Figure 5B, Supplemental Table S16). Additionally, for upregulated proteins in the PPI network, four terms were significantly involved in the worker including ribosome (q-value = 6.4×10^{-22}), chromatin organization (q-value = 4.3×10^{-3}), programmed cell death (q-value = 9.5×10^{-3}), and axonogenesis (q-value = 2.1×10^{-2}) (Figure 6B). Eight terms were significantly enriched in the drone such as ubiquitin-dependent protein catabolic process (q-value = 2.8×10^{-7}), cellular response to DNA damage stimulus (q-value = 2.8×10^{-7}), programmed cell death (q-value = 6.6×10^{-7}), oocyte differentiation (q-value = 1.1×10^{-6}), cell proliferation (q-value = 1.3×10^{-4}), compound eye development (q-value = 8.4×10^{-4}), antioxidant activity (q-value = 1.1×10^{-3}), and tRNA aminoacylation (q-value = 5.8×10^{-3}) (Figure 6E).

3.4. Proteome Difference between the Worker and Drone at 72 h

At the last stage of embryogenesis, 2304 proteins were expressed by the worker (1903) and drone (1838) (Figure S3C, Supplemental Tables S5 and S17). Of the 1437 shared proteins (62%), they were enriched 13 biological pathways such as ribosome, citrate cycle, proteasome, wnt signaling pathway, and circadian rhythm (Figure 4C, Supplemental Tables S9 and S18). Four pathways were uniquely enriched in the worker: arginine and proline metabolism ($p = 3.4 \times 10^{-2}$), β-alanine metabolism ($p = 4.9 \times 10^{-2}$), dorsal−ventral axis formation ($p = 4.0 \times 10^{-2}$), and hedgehog signaling pathway ($p = 2.4 \times 10^{-4}$). No pathway was exclusively enriched in the drone (Figure 4C, Supplemental Tables S9 and S18). By comparing the functional classes, the worker embryo expressed more proteins related to cytoskeleton and morphogenesis and fewer proteins associated with cell cycle control/apoptosis than those in the drone (Figure S4C, Supplemental Tables S5 and S17). Quantitatively, 91 proteins (54 were upregulated in worker and 37 in drone) were differentially expressed (fold change ≥ 2 and $p < 0.05$) between the two embryos (Figure 5C, Supplemental Table S19). The upregulated proteins in the worker were associated with lipid metabolism, morphogenesis, transcription, translation, and transporter. The proteins with high level of expression in the drone were mainly implicated in antioxidation/defense. For the upregulated proteins in PPI network of the worker, they were mainly related to spindle organization (q-value = 9.3×10^{-3}), ribosome biogenesis (q-value = 1.8×10^{-2}), and positive regulation of the biosynthetic process (q-value = 2.4×10^{-2}), whereas cellular response to lipid (q-value = 4.7×10^{-5}) and oxygen-containing compounds (q-value = 9.8

DOI: 10.1021/acs.jproteome.5b00625
J. Proteome Res. XXXX, XXX, XXX−XXX

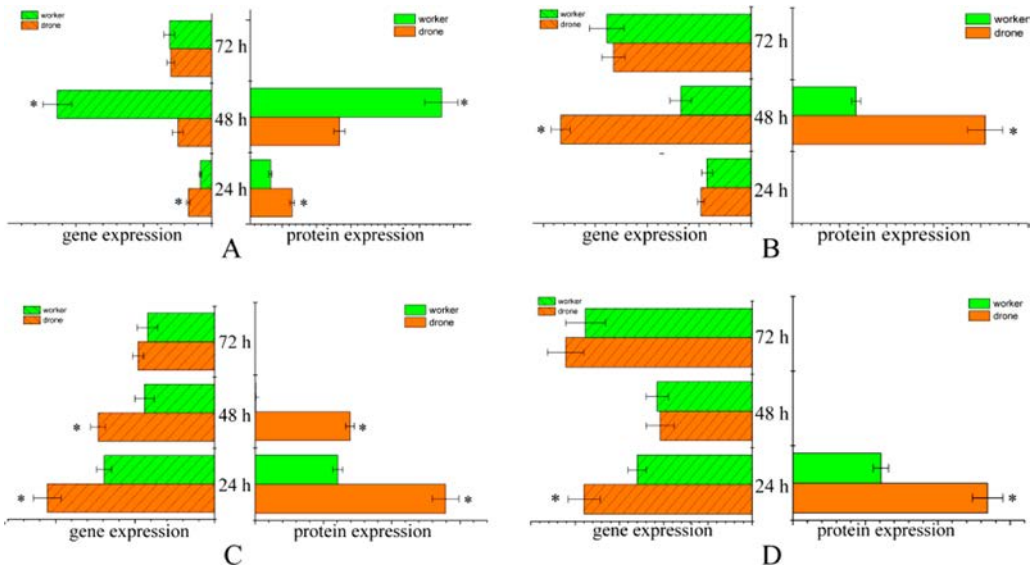

Figure 7. A test of the differentially expressed (fold change ≥ 2 and $p < 0.05$) proteins at the mRNA level by quantitative real-time PCR analysis. The gene expression is normalized with the reference gene (GAPDH). The color bars represent the relative expression values of mRNA and proteins in differently aged embryos. Abbreviated protein names indicate different proteins as in Supplemental Table S1. Panels A–D show the expression trends of RpL36, Lach, janA, and Mael, respectively. The error bar is standard deviation. The asterisks show significant differences ($p < 0.05$).

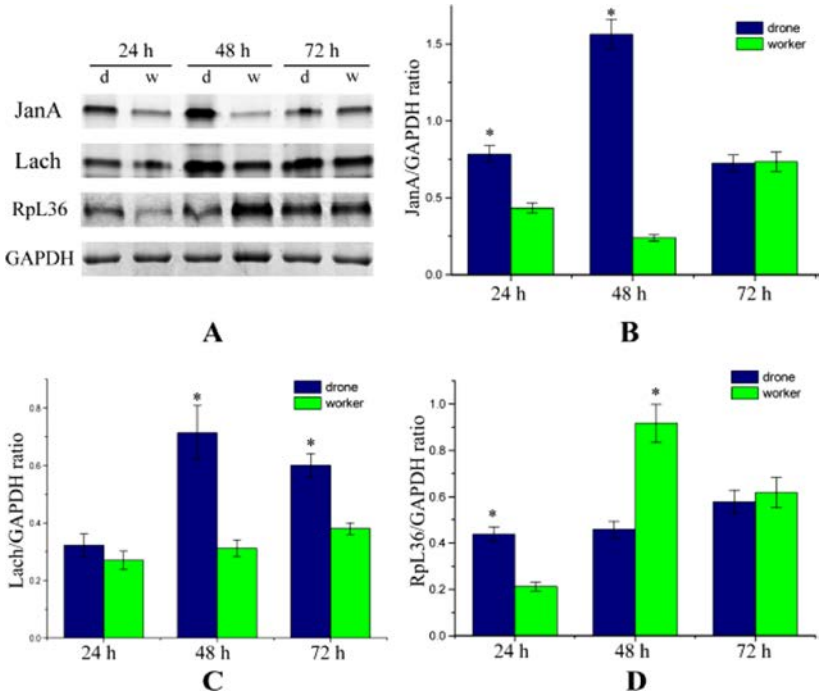

Figure 8. Western-Blotting analysis of sex-regulated protein janus-A-like (janA), lachesin-like isoform X1 (Lach), and 60S ribosomal protein L36 (RpL36). The protein samples from worker (w) and drone (d) embryos (*A.m.ligustica*) are subjected to SDS-PAGE followed by Western-Blotting analysis. JanA, Lach, and RpL36 are detected using the corresponding polyclonal antibodies. GAPDH is used as reference control. (A) The Western-Blotting bands of janA, Lach, RpL36, and GAPDH. (B–D) The relative expression values of janA, lach, and RpL36 in the honeybee (*A.m.ligustica*) worker and drone at the three stages (normalized by GAPDH). The error bar is standard deviation. The asterisks show significant differences ($p < 0.05$).

$\times 10^{-3}$) were significantly enriched in the drone embryo (Figure 6C,F).

3.5. Verification

Among the 20 selected key proteins, 15 of them were observed with consistent tendency between the protein and gene expression, that is, RpL36, Lach, janA, protein maelstrom homologue (Mael), atlastin isoform X2 (Atl), tyrosine-protein phosphatase 69D (Ptp69D), mesencephalic astrocyte-derived neurotrophic factor homologue (Manf), eukaryotic translation initiation factor 4E (eIF-4E), programmed cell death protein 5 (Pdcd5), splicing factor 3B (SF3B), ubiquitin-conjugating enzyme E2 (UbcD2), importin subunit alpha (Pen), spectrin (Spec), glutaredoxin 3 (GLRX3), and 40S ribosomal protein S18 (RpS18) (Figure 7, Figure S5). Again, the abundance levels

DOI: 10.1021/acs.jproteome.5b00625
J. Proteome Res. XXXX, XXX, XXX–XXX

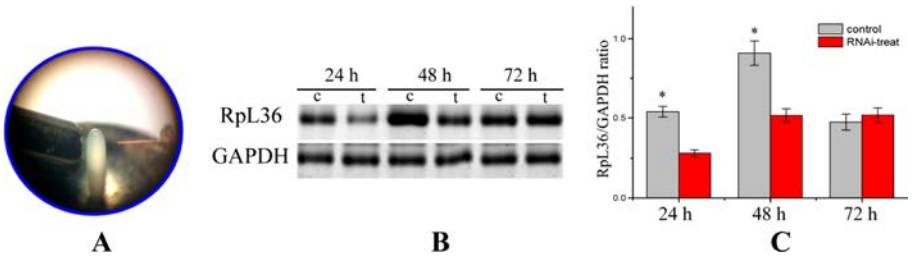

Figure 9. RNA interference induced knockdown of 60S ribosomal protein L36 (RpL36). (A) The dsRNA of gene RpL36 was injected at 2.5 $\mu g/\mu L$ in H_2O into freshly laid honeybee worker eggs (5 nL injected into each embryo), while an equal volume of sterile water was injected as a control. The injected embryos were incubated at 34 °C and 80% humidity and harvested at 24, 48, and 72 h. (B) Western-Blotting showing the RpL36 protein level in the worker embryo at three stages. (C) Quantitative real-time PCR showing the transcript-level RpL36 in the worker embryo at three stages. Letters "c" and "t" represent control and RNAi-treat, respectively. The error bar is standard deviation. The asterisks show significant differences ($p < 0.05$).

of RpL36, Lach, and janA of the proteomic data were verified by Western-Blotting analysis (Figure 8). The RNAi-induced knockdown of RpL36 showed a significantly reduced expression level in its encoding gene in the early to middle stage (24−48 h), but the expression of mRNA was resumed to the normal level in the 72 h embryo (Figure 9), which may be caused by the species-specific timeliness of RNAi.[40]

4. DISCUSSION

Unveiling the mechanism governing the drone bee embryogenesis and its difference with the worker is of vital importance for honeybee developmental biology. Employing state-of-the-art high-accuracy MS-based proteomics, 2788 and 2840 proteins were, respectively, identified in the worker and drone embryo, which make this the largest proteomic study hitherto conducted in honeybee embryo. Here, the embryonic proteome of the drone is the first large-scale and comprehensive documentation, whereas the proteome coverage of the worker embryo increases up to 20% the previously reported 1460 proteins.[25] The embryogenesis trajectory at the proteome level of the drone is generally similar to what is happening in the worker, meaning that the proteins expressed by the young embryo (24 h) are to prepare for metabolic energy for the subsequent organogenesis, and the proteins expressed by the middle to late staged embryo (48−72 h) are crucial for forming the basic embryo configuration and improving the construction of the rudimentary organs. However, wide scenarios of differences were found between the worker and drone by qualitative and quantitative proteome comparison of each embryonic stage. The pre-established differential genetic makeup between the worker and drone has evolved distinct proteome programs to sustain their respective embryonic development. The drone embryo on a whole displays an earlier morphogenesis than the worker because of its younger age. These observations have been supported by the enhanced expressed proteins and pathways related to morphogenesis, transcriptional, and translational machinery to tune the biological materials demanded for the organogenesis. Moreover, to match the temporal-difference of organogenesis, the worker and drone embryos employ distinct antioxidant mechanisms to remove the free radicals and secure their individual embryogenesis processes. Still, the drone embryo's strongly expressed cytoskeletal proteins imply their vital roles to support the large body size.

4.1. Drone Embryogenesis Generally Follows the Worker's Mode

Similar to the worker embryogenesis,[25] ~33% of the identified proteins were presented in all developmental stages of the drone embryos (Figure 1, Supplemental Tables S3−S5). These proteins were mainly related to translation, folding/degradation, transporter, and carbohydrate metabolism/energy (Figure S1), and involved in the metabolic pathways of ribosome, carbon metabolism, biosynthesis of amino acids, proteasome, and citrate cycle (Figure 2, Supplemental Tables S7−S9). These functional classes and pathways suggest their essential roles in driving embryogenesis by providing newly synthesized proteins and metabolic energy, which is consistant with the previous reports on the embryos of drone[22] and worker.[25] Matching with the unique physiology of differentially aged embryos, however, the drone embryo has its age-dependent proteomic characteristics. The overrepresented proteins in the 24 h implicated in the categories of carbohydrate metabolism and pathway of pyruvate, starch/sucrose, cysteine/methionine, and glyoxylate/dicarboxylate metabolism (Figure 2) are indicative of providing metabolic energy for zygote cleaving and early blastoderm forming.[25] The significantly enriched fatty acid degradation pathway (fatty acyl-CoA reductase, acetyl-CoA acetyltransferase, 2-hydroxyacyl-CoA lyase 1, and so on) further manifests the high-energy demand at this age as a driving force by fuelling the fatty compound such as vitellogenin and yolk protein.[25] Moreover, the significantly enriched category of cell maturation in the PPI network (Figure S2A) and over 100 morphogenesis related proteins expressed at this age (Supplemental Tables S3 and S6) indicate that the organogenesis at the molecular level occurs in advance of morphological changes, which agrees with the findings in the worker embryo.[25]

The 48 h is a vital time window for the formation of the basic embryo configuration by the accumulation of protein building blocks for the shaping of newly emerged organs.[1,41] This is supported by the significantly enriched biological pathways (Figure 2) and categories in the PPI network (Figure S2B) such as aminoacyl-tRNA biosynthesis, β-alanine metabolism, ribosome, oocyte development, and macromolecular complex assembly. All of these functional categories and biological pathways are fundamental for providing molecular building blocks to shape the newly emerged organs, which are also in line with the formation of rudimentary organs during the drone and worker embryogenesis.[25] Moreover, the highly activated wnt signaling pathway in the middle and late stages (Figure 2, Supplemental Table S8), functioning in embryonic cell

DOI: 10.1021/acs.jproteome.5b00625
J. Proteome Res. XXXX, XXX, XXX−XXX

proliferation, migration, fate specification, and body axis patterning, is suggestive of the key roles in proper formation of important tissues including heart and muscle during the embryogenesis.[42,43] Furthermore, an activated phototransduction pathway (Figure 2, Supplemental Table S8), which converts the signal of light (photons) into a change of membrane potential in photoreceptor cells,[44] is likely a response to the rudimentary formation of compound eyes or the optic nerve system that is important for the drone bees to catch and mate with virgin queens in the open air using their powerful optical system.[7] The enriched ubiquitin-dependent protein catabolic process and programmed cell death of the upregulated protein interaction network (Figure S2B), together with the activated phagocytosis pathway (Figure 2, Supplemental Table S8), are supposed to be involved in the process of the dorsal blastoderm apoptosis at the late blastoderm stage[1] or the degradation and reutilization of the incorrect configured polypeptides.[45,46] All of these observations make clear the notion that they are of functional importance concerning the rudimentary shaping of newly emerged organs for the formation of the basic configuration of drone embryo.

The last stage of embryogenesis develops further to improve the construction of the rudimentary organs.[41] This is achievable by the intensely involved biological pathways of RNA transport, pentose phosphate, and mRNA surveillance (Figure 2, Supplemental Table S9) to provide energy and biomaterials as in the 72 h worker embryo.[25] Of these, the strongly activated pathway of fatty acid degradation (Figure 2, Supplemental Table S9) underlines the high metabolic energy requirement of the old embryos supplied by the decomposition of available yolk[41] as in the early stage. Moreover, pathways of fatty acid degradation also might be involved in the organ formation (midgut and ventriculus) by depleting the enclosed yolk,[41] which coincides with the observation of the worker embryogenesis.[25] The circadian rhythm pathway (Figure 2, Supplemental Table S9) allows the organisms internal estimate of the external local time to program their activities at an appropriate time to act in concert with the daily environmental cycle.[47] Protein kinase shaggy isoforms, functioning in the circadian rhythm pathway, have been reported important for several developmental events such as embryonic segmentation, chaeta, and epithelial cell and heart development in *Drosophila*.[48,49] It is thus believed that the uniquely enriched circadian rhythm pathway at this age plays key roles in regulating establishment of the fine rudimentary organs.

As mentioned earlier, the honeybee worker and drone inherit completely different genetic settings and social roles in the colony.[3] These biological differences have made manifest in our data that proteins/genes and pathways change to program their embryogenesis process and are involved in a complex network of molecular events and reflected in the following points.

4.2. Worker and Drone Embryos Evolve Different Transcriptional and Translational Machinery To Prime Their Organogenesis

The integrated pipeline of transcription, translation, folding, and transporter is the indispensable machinery for protein maturation and assembling of the proteins for organs.[50] Transcription is the first step of gene expression, in which mRNA is being transcribed, and it in turn serves as a template for the synthesis of polypeptide chains through translation.[51] Then the nascent polypeptides later fold into an active protein and perform their functions in the cell,[52] for instance, the splicing factor involved in the removal of introns from strings of mRNA;[53] ribosomal proteins are responsible for catalyzing protein synthesis by functionality of a small 40S subunit and a large 60S subunit.[54] Protein disulfide-isomerase (PDI) is vital in cross-linking to nascent polypeptides and folding the disulfide-containing proteins.[55,56] The transporters in upstream peptide synthesis, such as nuclear pore complex protein, can carry mRNA to the cytoplasm,[57] and in the downstream are mainly to sort the newly synthesized proteins to specific intracellular locations.[58] They play key roles for forming the blastoderm, germ band, and the rudiment of embryonic organs in *Apis mellifera*[25,41] such as sorting nexin. The central significance of the above categories involved in transcriptional and translational machinery has reflected that they are overlapped by the proteomes in the worker and drone throughout the whole embryogenesis process (Supplemental Table S6). Interestingly, we observed that the highly expressed proteins implicated in transcriptional and translational machinery acted in concert with the enhanced expression of proteins related to morphological structure (Figure 5). This observation suggests that the protein synthesis is vital for the morpho-structural formation by acting as a protein building block to promote the organogenesis. However, the transcriptional and translational machinery related proteins in the worker and drone displayed quite distinct expression programs. At 24 h, the higher number of upregulated proteins involved in transcriptional and translational machinery in the drone than those in the worker emphasizes that stronger protein blocks is demanded by the drone embryogenesis at this young stage (Figure 5A, Supplemental Table S13). At the middle stage (48 h), the more strongly expressed ribosome subunits in the worker (Figure 6B) suggest that protein synthesis is still going on, while the highly induced ubiquitin-dependent protein catabolic process in the drone (Figure 6E) signifies that protein synthesis has reached the late stage of postsynthesis processing (protein folding or degradation). These differences in related proteins, RpL36, eIF-4E, RpS18, SF3B, Pen, and UbcD2, are further supported by their individual gene expressions (Figure 7, Figure S5). At the late stage, the upregulated proteins enriched in ribosome biogenesis and positive regulation biosynthetic in the worker (Figure 6C) manifest that the embryo still develop and maintain high demands to assemble blocks for the preparation of rudimentary organ formation. In all, the biological functions of transcriptional and translational machinery in the worker and drone embryogenesis as a whole evolve a distinct program for synthesis of protein blocks for the formation of rudimentary organs. The drone embryo develops an earlier demand for proteins as building blocks to promote the embryonic development than that in the worker.

4.3. Worker and Drone Embryos Have Time-Difference in Morphogenetic Occurrence

Morphogenesis is the key developmental process of forming the tissues and organs with well-ordered spatial arrangements.[41] For the honeybee embryo, the establishment of the rudimentary organs involves multiple processes of cell proliferation, differentiation, movement, adhesion, and induction.[1,41] The large number of highly expressed proteins implicated in morphogenesis of drone embryo at 24 h indicates that morphogenesis occurs earlier than in the worker (Figure 5A, Supplemental Table S13). For instance, Atl is the key regulator of muscle organ development and synaptic growth at neuromuscular junction;[59] Ptp69D has a key role in dendrite

DOI: 10.1021/acs.jproteome.5b00625
J. Proteome Res. XXXX, XXX, XXX−XXX

morphogenesis, axon guidance, and axonogenesis;[60] Manf is also involved in the development of neuron projections,[61] and the importance of the above proteins was supported by their expression at the gene level (Figure S5). Again, the strongly activated functional classes of macromolecular complex assembly, eukaryotic translation initiation factor 3 complex and neuron projection guidance in the PPI network in the 24 h drone embryo (Figure 6D), further support the fact the morphogenesis occurs in the drone is in advance of that in the worker. The early induced morphogenesis also has corroborated in the earlier analysis of proteins implicated in transcriptional and translational machinery.

Noticeably, the worker and drone embryos have evolved quite unique strategies to construct the rudimentary organs at 48 h. Although the numbers of morphogenesis proteins and the pathways in the two embryos were similar (Figure 4B, Supplemental Tables S4 and S14), they adapted a quite distinct complex network of molecular events to prime their embryogenesis. For the worker embryo, the significantly enriched pathway of circadian rhythm (Figure 4B, Supplemental Table S15) has been reported to be directly involved in the morphogenesis of chaeta, epithelium, and heart in *Drosophila*.[48,49,62] The significantly activated hedgehog signaling pathway (Figure 4B, Supplemental Table S15) is suggestive of a crucial role in regulating the development of a variety of tissues and organs as in *Drosophila*.[63,64] Moreover, the exclusively enriched pathway of dorsal−ventral axis formation (Figure 4B, Supplemental Table S15) suggests a role implicated in the specification of the embryonic body axes (another is the anterior−posterior axes), which is the key process of developing a program or blueprint for constructing the embryos and indicates the initiation of pattern formations in *Drosophila*.[65] Still, the enriched category-axonogenesis of the upregulated proteins in the PPI network of worker (Figure 6B) indicates that the embryo at this age is at the initial stage for tissues and organs formation.[66] In contrast, for the drone, the significantly enriched pathways of phototransduction and phagosome (Figure 4B, Supplemental Table S8) are indicative of the need for configuration of the nervous system and the apoptosis of dorsal blastoderm as in *Drosophila*,[44,67] which is supported by the validated gene (Pdcd5) expression related to this aspect (Figure S5). The significantly enriched functional category of compound eye development and tRNA aminoacylation in the PPI network (Figure 6E) indicates the key roles for the drone embryo to respond to its physiological demand of developing the big compound eye since it is powerful sense organ and functionally important for visual detection of virgin queens in the sky.[7] The large number of the morpho-structural proteins together with their elevated expression by the drone (Figure 5B, Figure S4, Supplemental Table S16) show that that the embryogenesis reaches a peak time in morphogenetic development, while the worker does not. For instance, the drone embryo strongly expressed the proteins Lach and janA, which function in the embryonic epithelium/heart morphogenesis[68] and regulate the process of sexual differentiation,[69] respectively, and their significance is also supported by their stronger gene expression (Figure 7).

When an embryo develops to 72 h, it is the major time frame of the morphogenesis occurrence in the worker embryos. The overrepresented and enhanced expression of the morphogenesis related proteins by the worker embryo suggest that 72 h is the high time of rudimentary organogenesis, which is line with our previous work.[25] In response to this, the pathways of dorsal−ventral axis formation[65] and hedgehog signaling pathway[63,64] were highly activated (Figure 4C, Supplemental Table S18), suggesting that the events of the pattern formation and embryonic cell differentiation are still ongoing actively. Also, it is further supported by the significantly enriched ribosome biogenesis and positive regulation of biosynthetic processes of the upregulated protein PPI network (Figure 6C), which is vital in providing biological material for the rudimentary organ building. In contrast, there were no exclusive pathways and a fewer number of highly expressed proteins associated with morphogenesis in the drone (Figures 4C and 5C; Supplemental Tables S9, S18, and S19), suggesting that its organogenesis has already reached a stage of the completeness of organogenesis, tissue elongation, and body segmentation. This observation indicates that drones may evolve a unique strategy of organogenesis to configure their large body size completely during embryogenesis by rescheduling the embryonic events via an earlier-start of morphogenesis and relatively longer developmental time (~3 h longer than worker).[70]

4.4. Enhanced Expression of Cytoskeletal Proteins in the Drone Embryo Matches with Its Large Body Size

The body size of the drone bees is ~3-times heavier than that of worker bees,[71] suggesting a larger cytoskeletal scaffold required to support their big body size. The cytoskeleton is a series of intercellular proteins that help a cell with shape, movement, and providing a scaffold to organize the contents of the cell in space.[72,73] During the whole process of embryonic development, the larger number and escalated expression of cytoskeleton proteins in the drone relative to the worker (Figure 5, Supplemental Tables S13, S16, and S19) suggest their vital constitutive roles for delivering substances or mediating an extended spatial distribution in response the large body size. The upregulated proteins enriched in a microtubule in the 24 h drone embryo (Figure 5A, Supplemental Table S13) indicate that the drone bees have high demand for scaffold materials to shape the specialized structures, segment the body, and organize the contents of the cell. Moreover, except for the role in the cytoskeleton organization, proteins in the cytoskeleton class also participate in the rudimentary establishment and tissue specification in *Drosophila*. For example, actin-interacting protein is involved in the differentiation of imaginal disc-derived wing hair,[74] protein maelstrom homologue takes part in the specification of oocyte anterior/posterior,[75] and Spec is related to the development of central nervous system and oocyte construction,[76] which is underscored by the strong expression of Mael and Spec at their genetic level (Figure 7, Figure S5).

4.5. Worker and Drone Employ Different Antioxidant Mechanism To Ensure the Embryogenesis

As in the other living organisms, the honeybee embryo has also developed a complex network of antioxidants to prevent oxidative damage to cellular components such as fatty acids, proteins, and nucleic acids, which are the main cellular components susceptible to damage by free radicals.[77−79] For the embryo at 24 h, the upregulated expression of the antioxidant class by the worker (Figure 5A, Supplemental Table S13), such as glutathione S-transferase omega-1, peroxiredoxin 1, and thioredoxin-2, may respond to the radical damages derived from the high metabolic activity of fatty acid, by which the lipid is mobilized and fueled for energy preparation.[2,41] At the middle and late stage, the large number of antioxidant proteins with high levels of expression by drones

DOI: 10.1021/acs.jproteome.5b00625
J. Proteome Res. XXXX, XXX, XXX−XXX

(Figure 5B, Figure S4B), such as catalase, mucin-5AC isoform 1, superoxide dismutase 1, and GLRX3 (gene expression supported, Figure S5), is supposed to be functionally important to eliminate the free radicals produced by the active organogenesis of the embryo at these ages. The vital role of antioxidants is also reflected by their significant enrichment (antioxidant activity and cellular response to oxygen-containing compound) in the PPI network of the drone embryo at 48 and 72 h. These observations suggest that the worker and drone embryos employ a distinct antioxidant mechanism to fine-tune protein function for optimizing antioxidant activity that coincides with the most active time of the embryogenesis.

5. CONCLUSIONS

We identified 2788 and 2840 proteins in the embryo of worker and drone, respectively, across the three time-points. This represents an unprecedented depth of the proteome in the honeybee embryos and deciphers molecular mechanisms that regulate the drone embryogenesis and delaminate the mechanistic divergence between the worker and drone embryogenesis. Although the drone has a completely different genetic makeup from worker, the mode of its embryogenesis is on the whole similar to the worker's. The age-dependent proteome in the young embryo (<24 h) is primarily responsible with providing metabolic energy for organogenesis, and in the middle to late stage (48−72 h) to form the basic embryo configuration and construction of the rudimentary organs. However, the two embryos adapt a distinct proteome program to prime their respective embryogenesis. The morphogenetic occurrence in the drone embryo is earlier than that in the worker, and this is solidified by strongly expressed proteins and pathways implicated in transcriptional and translational machinery to support the needed protein materials for the organogenesis. Moreover, because of the temporal-difference of organogenesis, the worker and drone embryos employ distinct antioxidant mechanisms to remove the free radicals that match with the embryogenesis. In addition, to respond to the large body size, the drone bees strongly express cytoskeletal proteins in the embryos for good organization of shape, movement, and the contents of the cell. Moreover, the verified expression trend between protein and gene, and the successfully induced knockdown gene expression of RpL36 by RNAi during 24−48 h age of embryo, provide sound evidence for the further study into the gene function of the honeybee embryo at the proper time. This is important for honeybee embryology and other social insects. Our data significantly expand novel understanding of a range of regulatory mechanisms governing the embryonic development. Further knowledge gained through such a valuable resource has the potential to lead to major advances in this area.

■ ASSOCIATED CONTENT

Supporting Information

The Supporting Information is available free of charge on the ACS Publications website at DOI: 10.1021/acs.jproteome.5b00625.

Functional category of shared proteins; PPI network of the upregulated proteins; numbers of worker and drone proteins identified; comparison of the identified proteins; test of the differentially expressed proteins by quantitative real time PCR (PDF)

Primer sequences used for validatory real-time PCR; sequencing the honeybee gene of RpL36 cloned into vector Puc19 for RNAi; identification of expressed proteins; biological pathway enrichment of the identified proteins; expressional analysis of the differentially expressed proteins (XLSX)

■ AUTHOR INFORMATION

Corresponding Author

*E-mail: apislijk@163.com. Phone: +86 10 6259 1449. Fax: +86 10 6259 1449.

Notes

The authors declare no competing financial interest.

■ ACKNOWLEDGMENTS

Thank you to Katrina Klett for the help editing this manuscript. This work was supported by the Agricultural Science and Technology Innovation Program (CAAS-ASTIP-2015-IAR), earmarked fund for Modern Agro-industry Technology Research System (CARS-45).

■ REFERENCES

(1) DuPraw, E.. The honeybee embryo. In *Methods in Developmental Biology*; Crowell: New York, 1967; pp 183−217.
(2) Nelson, J. *The Embryology of the Honeybee*; Princeton University Press: Princeton, NJ, 1915; pp 56−143.
(3) Winston, M. L. *The Biology of the Honey Bee*; Harvard University Press: Cambridge, London, 1987; pp 32−189.
(4) Robinson, G. E. Regulation of division of labor in insect societies. *Annu. Rev. Entomol.* **1992**, *37*, 637−65.
(5) Robinson, G. E. Genomics and integrative analyses of division of labor in honeybee colonies. *Am. Nat.* **2002**, *160* (Suppl. 6), S160−72.
(6) Radloff, S. E.; Hepburn, H. R.; Koeniger, G. Comparison of flight design of Asian honeybee drones. *Apidologie* **2003**, *34*, 353−358.
(7) Seidl, R. Die Sehfelder und Ommatidien-Divergenzwinkel der drei Kasten der Honigbiene (*Apis mellifica*). *Verh. Dtsch. Zool. Ges.* **1980**, 367.
(8) Bergem, M.; Norberg, K.; Roseth, A.; Meuwissen, T.; Lien, S.; Aamodt, R. H. Chimeric honeybees (*Apis mellifera*) produced by transplantation of embryonic cells into pre-gastrula stage embryos and detection of chimerism by use of microsatellite markers. *Mol. Reprod. Dev.* **2006**, *73*, 475−81.
(9) Maleszka, J.; Foret, S.; Saint, R.; Maleszka, R. RNAi-induced phenotypes suggest a novel role for a chemosensory protein CSP5 in the development of embryonic integument in the honeybee (*Apis mellifera*). *Dev. Genes Evol.* **2007**, *217*, 189−96.
(10) Patel, A.; Fondrk, M. K.; Kaftanoglu, O.; Emore, C.; Hunt, G.; Frederick, K.; Amdam, G. V. The making of a queen: TOR pathway is a key player in diphenic caste development. *PLoS One* **2007**, *2*, e509.
(11) Kucharski, R.; Maleszka, J.; Foret, S.; Maleszka, R. Nutritional control of reproductive status in honeybees via DNA methylation. *Science* **2008**, *319*, 1827−30.
(12) Beisser, K.; Munz, E.; Reimann, M.; Renner-Müller, I. C. E. Experimentelle Untersuchungen zur in vitro-Kultivierung von Zellen der Kärntner Honigbiene (*Apis mellifera carnica Pollmann*, 1879). *J. Vet. Med., Ser. B* **1990**, *37*, 509−519.
(13) Kreissl, S.; Bicker, G. Dissociated neurons of the pupal honeybee brain in cell culture. *J. Neurocytol.* **1992**, *21*, 545−556.
(14) Gascuel, J.; Masson, C.; Bermudez, I.; Beadle, D. J. Morphological analysis of honeybee antennal cells growing in primary cultures. *Tissue Cell* **1994**, *26*, 551−558.
(15) Bergem, M.; Norberg, K.; Aamodt, R. M. Long-term maintenance of in vitro cultured honeybee (*Apis mellifera*) embryonic cells. *BMC Dev. Biol.* **2006**, *6*, 17.

DOI: 10.1021/acs.jproteome.5b00625
J. Proteome Res. XXXX, XXX, XXX−XXX

(16) Kitagishi, Y.; Okumura, N.; Yoshida, H.; Nishimura, Y.; Takahashi, J.; Matsuda, S. Long-term cultivation of in vitro Apis mellifera cells by gene transfer of human c-myc proto-oncogene. *In Vitro Cell. Dev. Biol.: Anim.* **2011**, *47*, 451−3.
(17) Chan, M. M.; Choi, S. Y.; Chan, Q. W.; Li, P.; Guarna, M. M.; Foster, L. J. Proteome profile and lentiviral transduction of cultured honey bee (*Apis mellifera* L.) cells. *Insect Mol. Biol.* **2010**, *19*, 653−8.
(18) Fleig, R.; Sander, K. Embryogenesis of the honeybee apis mellifera l. (hymenoptera: apidae): An sem study. *Int. J. Insect Morphol. Embryol.* **1986**, *15*, 449−462.
(19) Katzav-Gozansky, T.; Soroker, V.; Kamer, J.; Schulz, C. M.; Francke, W.; Hefetz, A. Ultrastructural and chemical characterization of egg surface of honeybee worker and queen-laid eggs. *Chemoecology* **2003**, *13*, 129−134.
(20) Woyke, J. Size change of Apis mellifera eggs during the incubation period. *J. Apicult Res.* **1998**, *37*, 239−246.
(21) Li, J.; Zhang, L.; Feng, M.; Zhang, Z.; Pan, Y. Identification of the proteome composition occurring during the course of embryonic development of bees (*Apis mellifera*). *Insect Mol. Biol.* **2009**, *18*, 1−9.
(22) Li, J.; Fang, Y.; Zhang, L.; Begna, D. Honeybee (*Apis mellifera ligustica*) drone embryo proteomes. *J. Insect Physiol.* **2011**, *57*, 372−84.
(23) Elsik, C. G.; Worley, K. C.; Bennett, A. K.; Beye, M.; Camara, F.; Childers, C. P.; de Graaf, D. C.; Debyser, G.; Deng, J.; Devreese, B.; Elhaik, E.; Evans, J. D.; Foster, L. J.; Graur, D.; Guigo, R.; teams, H. p.; Hoff, K. J.; Holder, M. E.; Hudson, M. E.; Hunt, G. J.; Jiang, H.; Joshi, V.; Khetani, R. S.; Kosarev, P.; Kovar, C. L.; Ma, J.; Maleszka, R.; Moritz, R. F.; Munoz-Torres, M. C.; Murphy, T. D.; Muzny, D. M.; Newsham, I. F.; Reese, J. T.; Robertson, H. M.; Robinson, G. E.; Rueppell, O.; Solovyev, V.; Stanke, M.; Stolle, E.; Tsuruda, J. M.; Vaerenbergh, M. V.; Waterhouse, R. M.; Weaver, D. B.; Whitfield, C. W.; Wu, Y.; Zdobnov, E. M.; Zhang, L.; Zhu, D.; Gibbs, R. A. Honey Bee Genome Sequencing, C., Finding the missing honey bee genes: lessons learned from a genome upgrade. *BMC Genomics* **2014**, *15*, 86.
(24) Hernandez, L. G.; Lu, B.; da Cruz, G. C.; Calabria, L. K.; Martins, N. F.; Togawa, R.; Espindola, F. S.; Yates, J. R.; Cunha, R. B.; de Sousa, M. V. Worker honeybee brain proteome. *J. Proteome Res.* **2012**, *11*, 1485−93.
(25) Fang, Y.; Feng, M.; Han, B.; Lu, X.; Ramadan, H.; Li, J. In-depth Proteomics Characterization of Embryogenesis of the Honey Bee Worker (*Apis mellifera ligustica*). *Mol. Cell. Proteomics* **2014**, *13*, 2306−20.
(26) Gala, A.; Fang, Y.; Woltedji, D.; Zhang, L.; Han, B.; Feng, M.; Li, J. Changes of proteome and phosphoproteome trigger embryo-larva transition of honeybee worker (*Apis mellifera ligustica*). *J. Proteomics* **2013**, *78*, 428−46.
(27) Jianke, L.; Mao, F.; Begna, D.; Yu, F.; Aijuan, Z. Proteome comparison of hypopharyngeal gland development between Italian and royal jelly producing worker honeybees (*Apis mellifera* L.). *J. Proteome Res.* **2010**, *9*, 6578−94.
(28) Feng, M.; Fang, Y.; Li, J. Proteomic analysis of honeybee worker (*Apis mellifera*) hypopharyngeal gland development. *BMC Genomics* **2009**, *10*, 645.
(29) Feng, M.; Fang, Y.; Han, B.; Zhang, L.; Lu, X.; Li, J. Novel aspects of understanding molecular working mechanisms of salivary glands of worker honeybees (*Apis mellifera*) investigated by proteomics and phosphoproteomics. *J. Proteomics* **2013**, *87*, 1−15.
(30) Woltedji, D.; Fang, Y.; Han, B.; Feng, M.; Li, R.; Lu, X.; Li, J. Proteome analysis of hemolymph changes during the larval to pupal development stages of honeybee workers (*Apis mellifera ligustica*). *J. Proteome Res.* **2013**, *12*, 5189−98.
(31) Bradford, M. M. A rapid and sensitive method for the quantitation of microgram quantities of protein utilizing the principle of protein-dye binding. *Anal. Biochem.* **1976**, *72*, 248−254.
(32) Zhang, J.; Xin, L.; Shan, B.; Chen, W.; Xie, M.; Yuen, D.; Zhang, W.; Zhang, Z.; Lajoie, G. A.; Ma, B. PEAKS DB: De Novo sequencing assisted database search for sensitive and accurate peptide identification. *Mol. Cell. Proteomics* **2012**, *11*, 11.
(33) Conesa, A.; Gotz, S.; Garcia-Gomez, J. M.; Terol, J.; Talon, M.; Robles, M. Blast2GO: a universal tool for annotation, visualization and analysis in functional genomics research. *Bioinformatics* **2005**, *21*, 3674−6.
(34) Xie, C.; Mao, X.; Huang, J.; Ding, Y.; Wu, J.; Dong, S.; Kong, L.; Gao, G.; Li, C.; Wei, L. KOBAS 2.0: a web server for annotation and identification of enriched pathways and diseases. *Nucleic Acids Res.* **2011**, *39*, W316−322.
(35) Warde-Farley, D.; Donaldson, S. L.; Comes, O.; Zuberi, K.; Badrawi, R.; Chao, P.; Franz, M.; Grouios, C.; Kazi, F.; Lopes, C. T.; Maitland, A.; Mostafavi, S.; Montojo, J.; Shao, Q.; Wright, G.; Bader, G. D.; Morris, Q. The GeneMANIA prediction server: biological network integration for gene prioritization and predicting gene function. *Nucleic Acids Res.* **2010**, *38*, W214−20.
(36) Eisen, M. B.; Spellman, P. T.; Brown, P. O.; Botstein, D. Cluster analysis and display of genome-wide expression patterns. *Proc. Natl. Acad. Sci. U. S. A.* **1998**, *95* (25), 14863−8.
(37) Saldanha, A. J. Java Treeview–extensible visualization of microarray data. *Bioinformatics* **2004**, *20*, 3246−8.
(38) Pfaffl, M. W. A new mathematical model for relative quantification in real-time RT-PCR. *Nucleic Acids Res.* **2001**, *29*, e45.
(39) Yu, F.; Mao, F.; Jianke, L. Royal jelly proteome comparison between A. mellifera ligustica and A. cerana cerana. *J. Proteome Res.* **2010**, *9*, 2207−15.
(40) Irie, N.; Sakai, N.; Ueyama, T.; Kajimoto, T.; Shirai, Y.; Saito, N. Subtype- and species-specific knockdown of PKC using short interfering RNA. *Biochem. Biophys. Res. Commun.* **2002**, *298*, 738−43.
(41) Fleig, R.; Sander, K. Embryogenesis of the honeybee Apis mellifera L. (Hymenoptera: Apidea): a SEM study. *Int. J. Insect Morphol. Embryol.* **1986**, *15*, 449−462.
(42) van Amerongen, R.; Nusse, R. Towards an integrated view of Wnt signaling in development. *Development* **2009**, *136*, 3205−14.
(43) Cadigan, K. M.; Nusse, R. Wnt signaling: a common theme in animal development. *Genes Dev.* **1997**, *11*, 3286−305.
(44) Hardie, R. C. Phototransduction in Drosophila melanogaster. *J. Exp Biol.* **2001**, *204*, 3403−9.
(45) Bilyy, R. O.; Shkandina, T.; Tomin, A.; Munoz, L. E.; Franz, S.; Antonyuk, V.; Kit, Y. Y.; Zirngibl, M.; Furnrohr, B. G.; Janko, C.; Lauber, K.; Schiller, M.; Schett, G.; Stoika, R. S.; Herrmann, M. Macrophages discriminate glycosylation patterns of apoptotic cell-derived microparticles. *J. Biol. Chem.* **2012**, *287*, 496−503.
(46) Rothman, S. How is the balance between protein synthesis and degradation achieved? *Theor. Biol. Med. Modell.* **2010**, *7*, 25.
(47) Dunlap, J. C.; Loros, J. J.; DeCoursey, P. J. *Chronobiology: Biological Timekeeping*; Sinauer Associates, Inc.: Sunderland, MA, 2004; pp 266.
(48) Ruel, L.; Pantesco, V.; Lutz, Y.; Simpson, P.; Bourouis, M. Functional significance of a family of protein kinases encoded at the shaggy locus in Drosophila. *EMBO J.* **1993**, *12*, 1657−69.
(49) Franco, B.; Bogdanik, L.; Bobinnec, Y.; Debec, A.; Bockaert, J.; Parmentier, M. L.; Grau, Y. Shaggy, the homolog of glycogen synthase kinase 3, controls neuromuscular junction growth in Drosophila. *J. Neurosci.* **2004**, *24*, 6573−7.
(50) Fedorov, A. N.; Baldwin, T. O. Cotranslational protein folding. *J. Biol. Chem.* **1997**, *272*, 32715−8.
(51) Hausner, W.; Thomm, M. Events during initiation of archaeal transcription: open complex formation and DNA-protein interactions. *J. Bacteriol.* **2001**, *183*, 3025−31.
(52) Anfinsen, C. B. The formation and stabilization of protein structure. *Biochem. J.* **1972**, *128*, 737−49.
(53) Chen, H. C.; Cheng, S. C. Functional roles of protein splicing factors. *Biosci. Rep.* **2012**, *32*, 345−59.
(54) Wool, I. G.; Chan, Y. L.; Gluck, A. Structure and evolution of mammalian ribosomal proteins. *Biochem. Cell Biol.* **1995**, *73*, 933−47.
(55) Klappa, P.; Freedman, R. B.; Zimmermann, R. Protein disulphide isomerase and a lumenal cyclophilin-type peptidyl prolyl cis-trans isomerase are in transient contact with secretory proteins during late stages of translocation. *Eur. J. Biochem.* **1995**, *232*, 755−64.
(56) Roth, R. A.; Pierce, S. B. In vivo cross-linking of protein disulfide isomerase to immunoglobulins. *Biochemistry* **1987**, *26*, 4179−82.

DOI: 10.1021/acs.jproteome.5b00625
J. Proteome Res. XXXX, XXX, XXX−XXX

(57) Roth, P.; Xylourgidis, N.; Sabri, N.; Uv, A.; Fornerod, M.; Samakovlis, C. The Drosophila nucleoporin DNup88 localizes DNup214 and CRM1 on the nuclear envelope and attenuates NES-mediated nuclear export. *J. Cell Biol.* **2003**, *163*, 701−6.
(58) Kanner, E. M.; Friedlander, M.; Simon, S. M. Co-translational targeting and translocation of the amino terminus of opsin across the endoplasmic membrane requires GTP but not ATP. *J. Biol. Chem.* **2003**, *278*, 7920−6.
(59) Lee, M.; Paik, S. K.; Lee, M. J.; Kim, Y. J.; Kim, S.; Nahm, M.; Oh, S. J.; Kim, H. M.; Yim, J.; Lee, C. J.; Bae, Y. C.; Lee, S. Drosophila Atlastin regulates the stability of muscle microtubules and is required for synapse development. *Dev. Biol.* **2009**, *330*, 250−62.
(60) Wollscheid, B.; Bausch-Fluck, D.; Henderson, C.; O'Brien, R.; Bibel, M.; Schiess, R.; Aebersold, R.; Watts, J. D. Mass-spectrometric identification and relative quantification of N-linked cell surface glycoproteins. *Nat. Biotechnol.* **2009**, *27*, 378−86.
(61) Palgi, M.; Lindstrom, R.; Peranen, J.; Piepponen, T. P.; Saarma, M.; Heino, T. I. Evidence that DmMANF is an invertebrate neurotrophic factor supporting dopaminergic neurons. *Proc. Natl. Acad. Sci. U. S. A.* **2009**, *106*, 2429−34.
(62) Konopka, R. J.; Benzer, S. Clock mutants of Drosophila melanogaster. *Proc. Natl. Acad. Sci. U. S. A.* **1971**, *68*, 2112−6.
(63) Nusslein-Volhard, C.; Wieschaus, E. Mutations affecting segment number and polarity in Drosophila. *Nature* **1980**, *287*, 795−801.
(64) Mohler, J. Requirements for hedgehog, a segmental polarity gene, in patterning larval and adult cuticle of Drosophila. *Genetics* **1988**, *120*, 1061−72.
(65) Rivera-Pomar, R.; Jãckle, H. From gradients to stripes in Drosophila embryogenesis: filling in the gaps. *Trends Genet.* **1996**, *12*, 478−483.
(66) Hidalgo, A.; Booth, G. E. Glia dictate pioneer axon trajectories in the Drosophila embryonic CNS. *Development* **2000**, *127*, 393−402.
(67) Zhou, Z.; Yu, X. Phagosome maturation during the removal of apoptotic cells: receptors lead the way. *Trends Cell Biol.* **2008**, *18*, 474−85.
(68) Karlstrom, R. O.; Wilder, L. P.; Bastiani, M. J. Lachesin: an immunoglobulin superfamily protein whose expression correlates with neurogenesis in grasshopper embryos. *Development* **1993**, *118*, 509−22.
(69) Yanicostas, C.; Ferrer, P.; Vincent, A.; Lepesant, J. A. Separate cis-regulatory sequences control expression of serendipity beta and janus A, two immediately adjacent Drosophila genes. *Mol. Gen. Genet.* **1995**, *246*, 549−60.
(70) Harbo, J. R.; Bolten, A. B. Development times of male and female eggs of the honey bee. *Ann. Entomol. Soc. Am.* **1981**, *74*, 504−506.
(71) Straus, J. Die chemische Zusammensetzung der Arbeitsbienen und Drohnen während ihrer verschiedenen Entwicklungsstadien. *Z. Biol.* **1911**, *56*, 347−397.
(72) Fletcher, D. A.; Mullins, R. D. Cell mechanics and the cytoskeleton. *Nature* **2010**, *463*, 485−92.
(73) Wickstead, B.; Gull, K. The evolution of the cytoskeleton. *J. Cell Biol.* **2011**, *194*, 513−25.
(74) Ren, N.; Charlton, J.; Adler, P. N. The flare gene, which encodes the AIP1 protein of Drosophila, functions to regulate F-actin disassembly in pupal epidermal cells. *Genetics* **2007**, *176*, 2223−34.
(75) Clegg, N. J.; Frost, D. M.; Larkin, M. K.; Subrahmanyan, L.; Bryant, Z.; Ruohola-Baker, H. Maelstrom is required for an early step in the establishment of Drosophila oocyte polarity: posterior localization of grk mRNA. *Development* **1997**, *124*, 4661−71.
(76) Pesacreta, T. C.; Byers, T. J.; Dubreuil, R.; Kiehart, D. P.; Branton, D. Drosophila spectrin: the membrane skeleton during embryogenesis. *J. Cell Biol.* **1989**, *108*, 1697−709.
(77) Sies, H. Oxidative stress: oxidants and antioxidants. *Exp Physiol* **1997**, *82*, 291−5.
(78) Vertuani, S.; Angusti, A.; Manfredini, S. The antioxidants and pro-antioxidants network: an overview. *Curr. Pharm. Des.* **2004**, *10*, 1677−94.
(79) Blokhina, O.; Virolainen, E.; Fagerstedt, K. V. Antioxidants, oxidative damage and oxygen deprivation stress: a review. *Ann. Bot.* **2003**, *91*, 179−94.

DOI: 10.1021/acs.jproteome.5b00625
J. Proteome Res. XXXX, XXX, XXX−XXX